Chinese Chemical Letters 33 (2022) 2906–2910

Contents lists available at ScienceDirect

Chinese Chemical Letters

journal homepage: www.elsevier.com/locate/cclet

Cu-embedded porous Al_2O_3 bifunctional catalyst derived from metal–organic framework for syngas-to-dimethyl ether

Yongle Guo[a,1], Lu Feng[b,c,1], Yuefeng Liu[b], Zhongkui Zhao[a,*]

[a] State Key Laboratory of Fine Chemicals, Department of Catalysis Chemistry and Engineering, School of Chemical Engineering, Dalian University of Technology, Dalian 116024, China
[b] Dalian National Laboratory for Clean Energy (DNL), Dalian Institute of Chemical Physics, Chinese Academy of Science, Dalian 116023, China
[c] Zhang Dayu School of Chemistry, Dalian University of Technology, Dalian 116024, China

ARTICLE INFO

Article history:
Received 11 August 2021
Revised 19 September 2021
Accepted 14 October 2021
Available online 22 October 2021

Keywords:
Dimethyl ether
CO hydrogenation
Bifunctional catalyst
Embedding-type structure
Metal–organic framework

ABSTRACT

Dimethyl ether (DME), as a promising alternative to diesel fuel and liquefied petroleum gas, has attracted considerable attention in catalysis domain. The catalytic direct synthesis of DME from syngas is an up-and-coming route but remains a challenge. In this work, we firstly prepared a Cu-embedded porous Al_2O_3 bifunctional catalyst (Cu@Al_2O_3-dp) by filling Cu-1,3,5-benzenetricarboxylate metal–organic framework (Cu-BTC MOF) with $Al(OH)_3$ followed by a two-step calcination process (400 °C for 4 h and 600 °C for 1 h), exhibiting excellent catalytic performance for direct synthesis of DME from syngas. Cu@Al_2O_3-dp catalyst demonstrates much higher CO conversion (25.7% *vs.* 15.4%) and extremely higher DME selectivity (90.4% *vs.* 63.9%) with the increased catalytic stability compared to the supported Cu catalyst on MOF-derived porous Al_2O_3 (Cu/Al_2O_3) prepared by incipient wetness impregnation method, ascribed to the unique embedding-type structure, promoted Cu dispersion and stronger metal-support interaction. This work not only provides an efficient syngas-to-DME catalyst, but also paves a new way for designing highly-efficient core-shell bifunctional catalysts for diverse consecutive reactions.

Dimethyl ether (DME), as the simplest ether without C–C bond, is expected to replace diesel due to its high cetane number and low toxicant emission. In addition, DME is also attractive as an excellent substitute for liquefied petroleum gases because of its similar physicochemical properties [1,2]. Traditionally, the production of DME is realized by a two-step method. To be more specific, firstly, the methanol is synthesized from syngas over the Cu-based catalysts, and then DME is produced by methanol dehydration over the solid acid catalysts [3,4]. Compared with the two-step synthesis of DME, the direct one-step syngas-to-DME (STD) reaction possesses many advantages, such as breaking the thermodynamic equilibrium limitation of methanol synthesis from syngas, promoting the production of DME and decreasing cost for DME producing, *etc.* [5,6]. For these reasons, the one-step STD reaction has drawn increasingly attention of worldwide researchers [7,8].

The commonly applied bifunctional catalyst in the STD reaction is a mixed catalyst, which is prepared by physically mixing methanol synthesis catalyst and methanol dehydration catalyst [9,10]. The component of methanol synthesis in the STD reaction is mainly Cu-based catalyst [11,12], and that of methanol dehydration in the STD reaction is solid acid catalyst, such as acidic zeolites [13,14] or γ-Al_2O_3 [15,16]. The preparation of mixed catalysts is simple, but there are still some disadvantages. For instance, long distance and random distribution of two active units result in low activity and selectivity. The supported dual-function catalysts can make up for the deficiency [17,18]. The components for methanol dehydration, such as zeolites or γ-Al_2O_3, have large specific surface areas and well-developed pores. As a support, it can promote the dispersion of active sites of methanol synthesis and improve the utilization of Cu [19,20]. However, the opening structure of supported catalysts lowers the selectivity of DME in the STD process. The core-shell capsule-structure catalyst is developed to solve the problem [6,21-27]. The closing-structured capsule-catalysts are prepared by coating the solid acid catalysts (zeolites or Al_2O_3) shell over the outer surface of millimetre-sized Cu-ZnO-Al_2O_3 cores [21–24]. The selectivity of DME over the capsule-catalyst is markedly higher than that over the open-structure bifunctional catalysts, such as hybrid catalysts and supported catalysts. A high-selectivity CuZn@m-Al_2O_3 catalyst for DME synthesis from syngas was also prepared by implanting the Cu-Zn nanoparticles into the matrix of mesoporous alumina [25]. However, the catalytic activity and

* Corresponding author.
E-mail address: zkzhao@dlut.edu.cn (Z. Zhao).
[1] These authors contributed equally to this work.

https://doi.org/10.1016/j.cclet.2021.10.031
1001-8417/

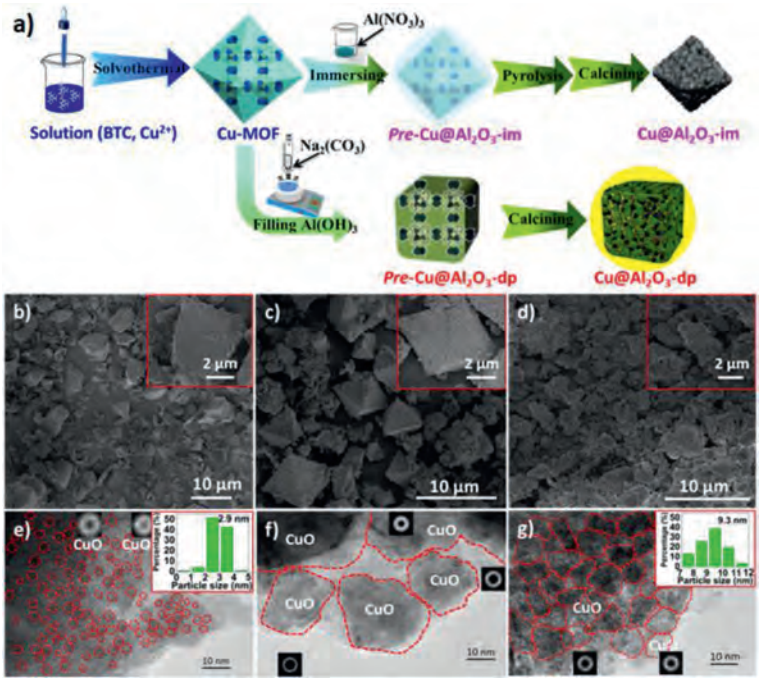

Fig. 1. (a) Schematic illustration of the synthesis of catalyst. SEM images of Cu@Al_2O_3-dp (b), Cu@Al_2O_3-im (c) and Cu/Al_2O_3 (d). Transmission electron microscope (TEM) images of Cu@Al_2O_3-dp (e), Cu@Al_2O_3-im (f) and Cu/Al_2O_3 (g).

the utilization efficiency of copper are very unsatisfactory owing to the use of the millimetre-sized Cu-based particles or poorly-dispersed Cu-based nanoparticles as methanol synthesis unit. It can be envisioned that an excellent bifunctional STD catalyst with high activity, Cu utilizing efficiency and high selectivity can be prepared with the highly-dispersed Cu nanoparticles embedded into porous Al_2O_3, and the high selectivity results from well-organized embedding-type structure. Metal–organic frameworks (MOFs) are widely used in gas storage, ion exchange and catalysis [28–31], due to its regular crystalline structure and developed porosity. Especially, the Cu-1,3,5-benzenetricarboxylate framework (Cu-BTC MOF) has also been widely applied to synthesize metal oxides, carbon nanodots, metal oxides@silica oxide and films [32–36], owing to its simple synthesis process, cheap reactants, high metal dispersion, ordered pores and large surface areas.

In this work, we, for the first time, prepared a new bifunctional catalyst (Cu@Al_2O_3-dp) with Cu implanted into porous Al_2O_3, derived from Cu-1,3,5-benzenetricarboxylate framework (Cu-BTC MOF) by filling MOF with Al_2O_3 using deposition-precipitation method with sodium carbonate solution as the precipitant (Fig. 1a). According to the SEM images and XRD pattern of Cu-BTC shown in Fig. S1 (Supporting information), the Cu-BTC MOF has been successfully synthesized by solvothermal method [10]. From results of N_2 adsorption shown in Fig. S2 (Supporting information), the Cu-BTC MOF contains abundant micropore. After filling MOF with aluminium, the uncalcined precursor of Cu@Al_2O_3-dp (pre-Cu@Al_2O_3-dp) barely has micropore, it may be ascribed to the fully-filled pore by aluminium, indicating aluminium infiltrate into the pore of MOF. In addition, in order to investigate the implanting ways of alumina and the effect of alumina on the catalyst structure and catalytic performance in the STD reaction, the Cu@Al_2O_3-im catalyst was prepared with immersion method where aluminium nitrate solution was used to fill Cu-BTC MOF. From the scanning electron microscope (SEM) images shown in Figs. 1b and c, the Cu@Al_2O_3-dp catalyst shows an irregular cube with the sizes ranging from 5 μm to 10 μm, and the Cu@Al_2O_3-im catalyst features an octahedral structure similar to Cu-BTC MOF, but the sizes are similar to that of Cu@Al_2O_3-dp and smaller than that of Cu-BTC MOF. From Table 1, the actual CuO loadings of Cu@Al_2O_3-dp and Cu@Al_2O_3-im catalysts are 13.0% and 92.9%, respectively. It is suggested that a little alumina is filled within Cu-BTC MOF by the immersion method. In order to clearly show the advantages of the implanting-type catalyst, the supported Cu catalyst on MOF-derived porous Al_2O_3 (Cu/Al_2O_3) was prepared by incipient wetness impregnation (IWI) method (Figs. 1d). The MOF-derived Al_2O_3 (Al_2O_3-DMOF) was obtained by repeatedly etching away the CuO component of the Cu@Al_2O_3-dp catalyst with ammonia water. Since a small amount of CuO in Al_2O_3-DMOF was completely and tightly wrapped by alumina, therefore, it was not dissolved by ammonia water, with the loading of CuO 4.2% (Table S1 in Supporting information). From Tables S1 and S2 (Supporting information), since there is a little exposed surface Cu site in Al_2O_3-DMOF (29.3 μmol/g) and it exhibits poor catalytic performance, the CuO loading similar to the Cu@Al_2O_3-dp catalyst is loaded onto Al_2O_3-DMOF, and the actual CuO loading of Cu/Al_2O_3 is 18.8%. Moreover, from Fig. 1g, it can be clear that there are many small particles accumulated on the outer surface of Cu/Al_2O_3 catalyst.

The microstructure of Cu@Al_2O_3-dp, Cu@Al_2O_3-im and Cu/Al_2O_3 catalysts are illustrated by high resolution transmission electron microscope (HRTEM) images in Figs. 1e-g, from which, it can be seen that the average size of CuO nanoparticles (NPs) of Cu@Al_2O_3-dp is 2.9 nm, which is far smaller than that of Cu/Al_2O_3 (9.3 nm) and Cu@Al_2O_3-im (20–40 nm). Furthermore, compared with intimate contact between CuO NPs of Cu/Al_2O_3 catalyst, the CuO NPs of Cu@Al_2O_3-dp catalyst are separated by Al_2O_3. Although the CuO NPs of Cu@Al_2O_3-im catalyst are separated by thin alumina, the CuO NPs aggregation are very severe, because of too little alumina to disperse CuO NPs and inhibit thermal sintering of CuO NPs. In addition, as shown in Table 1, the amount of exposed Cu active sites on Cu@Al_2O_3-dp catalyst (416.3 μmol/g) is larger than those of the Cu@Al_2O_3-im (105.7 μmol/g) and Cu/Al_2O_3 catalyst (341.5 μmol/g), although Cu@Al_2O_3-dp catalyst has a lower CuO loading. These results confirm that

Table 1
Characterization results of the $Cu@Al_2O_3$-dp, $Cu@Al_2O_3$-im and Cu/Al_2O_3 catalysts.

Catalyst	W_{CuO}[a] (%)	S_{micro}[b] (m^2/g)	S_{meso}[c] (m^2/g)	V_{micro}[b] (m^2/g)	V_{meso}[d] (mL/g)	n_{Cu}[e] (μmol/g)	n_a[f] (μmol/g)	D_{Cu}[g] (%)	$I_{Cu^+}/I_{Cu^{2+}}$[h]
$Cu@Al_2O_3$-dp	13.0	191	36	0.18	0.29	416.3	289.7	25.5	0.5
$Cu@Al_2O_3$-im	92.9	0	4	0	0.14	105.7	2.8	0.9	0.3
Cu/Al_2O_3	18.8	147	55	0.10	0.28	341.5	301.4	14.5	–

[a] Mass fraction of CuO, determined by ICP.
[b] *t*-plot.
[c] $S_{meso} = S_{BET} - S_{micro}$.
[d] BJH from adsorption branch.
[e] Amount of surface active Cu, determined by N_2O titration.
[f] Amount of acid sites, measured by NH_3 temperature-programmed desorption (NH_3-TPD).
[g] Cu dispersion, defined as the amount of surface active Cu divided by the total number of Cu atoms in the catalyst.
[h] The intensity ratio $I_{Cu^+}/I_{Cu^{2+}}$, calculated using the intensity of the Cu^+ peak divided by that of the Cu^{2+} peak from by deconvoluting the Cu $2p_{3/2}$ peak.

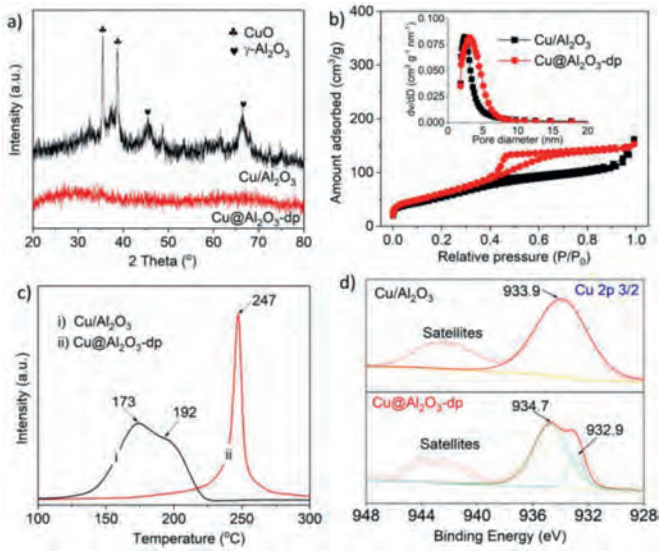

Fig. 2. XRD patterns (a), nitrogen adsorption-desorption isotherms and pore size distributions from adsorption branch (b), H_2-TPR profiles (c), and Cu 2p XPS spectra (d) of the Cu/Al_2O_3 and $Cu@Al_2O_3$-dp catalysts.

$Cu@Al_2O_3$-dp catalyst has a higher Cu dispersion. Additionally, the embedding type structure of $Cu@Al_2O_3$-dp may compress the CuO sintering during the calcination at high temperature in the preparation process, which may partially lead to its smaller CuO NPs compared to Cu/Al_2O_3. In order to verify the conjecture, the $Cu@Al_2O_3$-dp-400 and Cu/Al_2O_3-400 catalysts were prepared, and the preparation are similar to that of $Cu@Al_2O_3$-dp and Cu/Al_2O_3, and the only difference is that the former did not be calcined at 600 °C for 1 h. The exposed surface Cu sites of $Cu@Al_2O_3$-dp-400 and Cu/Al_2O_3-400 catalysts are shown in Table S1. From Table 1 and Table S1, it can be seen that the high temperature treatment is necessary for $Cu@Al_2O_3$-dp, which makes the Cu sites increase obviously from 97.0 μmol/g to 416.3 μmol/g, while the Cu sites of Cu/Al_2O_3 catalyst sinters severely and decreases from 611.8 μmol/g to 341.5 μmol/g. It is clear that the embedding type structure of $Cu@Al_2O_3$-dp may inhibit the sintering of CuO.

X-ray diffraction (XRD) was applied to further investigate the crystal structure of catalysts. From Fig. 2a and Fig. S3a (Supporting information), compared with Cu/Al_2O_3 and $Cu@Al_2O_3$-im catalysts with the obvious and sharp diffraction peaks of CuO (PDF#48-1548) [37], $Cu@Al_2O_3$-dp catalyst has no diffraction peaks of CuO, which shows its smaller grain size and higher dispersion and it agrees with the results of HRTEM and amount of surface active Cu. It is favourable for improving the CO conversion. The results of N_2 adsorption are shown in Fig. 2b, Fig. S3b (Supporting information) and Table 1, the adsorption–desorption isotherms and pore size distributions of $Cu@Al_2O_3$-dp and $Cu@Al_2O_3$ catalysts (Fig. 2b) display that both catalysts contain many micropores and mesopores, and the pores size of $Cu@Al_2O_3$-dp catalyst is larger than that of Cu/Al_2O_3. The types of hysteresis loop of $Cu@Al_2O_3$-dp and Cu/Al_2O_3 indicate the pores of the former resemble ink-bottle pores in alumina, while that of the latter is more likely to be intercrystalline pore [38]. From Table 1, the values of S_{micro} and V_{micro} of $Cu@Al_2O_3$-dp are higher than those of Cu/Al_2O_3. Although the $Cu@Al_2O_3$-dp has a slightly lower mesoporous surface area compared with Cu/Al_2O_3, which is owing to the more intercrystalline pore of Cu/Al_2O_3, the total surface area of $Cu@Al_2O_3$-dp is larger than that of Cu/Al_2O_3. From Fig. S3b and Table 1, it can be seen that the $Cu@Al_2O_3$-im nearly has neither micropore nor mesopore, which might be ascribed to the fully-filled structure.

H_2 temperature-programmed reduction (H_2-TPR) and X-ray photoelectron spectroscopy (XPS) experiments were conducted to study the reduction behaviour of CuO and metal-support interaction between Cu and alumina of catalysts. From Fig. 2c and Fig. S3c (Supporting information), compared with Cu/Al_2O_3 and $Cu@Al_2O_3$-im catalysts obviously with two kinds of reduction peaks of CuO, corresponding to the surface and bulk of reducible CuO species [24], only one main symmetrical reduction peak at 247 °C is found on $Cu@Al_2O_3$-dp catalyst, indicating homogenous distribution of CuO nanoparticles embedded in alumina [25]. From Fig. 2d and Fig. S3d (Supporting information), the Cu $2p_{3/2}$ peaks of $Cu@Al_2O_3$-dp and $Cu@Al_2O_3$-im catalysts can fitted and divided into two peaks at 932.9 and 934.7 eV, 932.7 and 933.7 eV, respectively, corresponding to Cu^+ and Cu^{2+} species. The Cu^+ species is ascribed to the Cu^{2+} reduced by decomposition of benzoate ligands during calcination [34], which can strengthen the CO adsorption and are beneficial to methanol synthesis [37]. From Table 1, the $I_{Cu^+}/I_{Cu^{2+}}$ intensity ratios of $Cu@Al_2O_3$-dp are higher that of the $Cu@Al_2O_3$-im. CO temperature programmed desorption (CO-TPD) profiles were shown in Fig. S4 (Supporting information), it can be seen that much stronger adsorbed CO on $Cu@Al_2O_3$-dp than that on Cu/Al_2O_3. Both indicate the capacity of CO adsorption on $Cu@Al_2O_3$-dp is stronger than that on $Cu@Al_2O_3$-im and Cu/Al_2O_3.

The binding energies of deconvolution peaks belonged to Cu^{2+} species on $Cu@Al_2O_3$-dp, Cu/Al_2O_3 and $Cu@Al_2O_3$-im catalysts are 934.7, 933.9 and 933.7 eV, respectively, which demonstrates the $Cu@Al_2O_3$-dp catalyst possesses stronger Cu-Al interaction compared to Cu/Al_2O_3 and $Cu@Al_2O_3$-im catalysts, which can improve intrinsic activity of Cu actives in the $Cu@Al_2O_3$-dp and conduces to the CO conversion [7].

The acidic nature of the catalysts is measured by NH_3-TPD experiments and shown in Table 1 and Fig. S5 (Supporting information). It can be seen that there are two main NH_3 desorption peaks in $Cu@Al_2O_3$-dp and Cu/Al_2O_3 catalysts. One was at low temperature (about 150–300 °C), corresponding to the desorption of the adsorbed NH_3 on weak acid sites, and the other was high temper-

Table 2
Catalytic performance of the Cu@Al_2O_3-dp, Cu@Al_2O_3-im, Cu/Al_2O_3 and Cu@Al_2O_3-com catalysts for DME direct synthesis from syngas.[a]

Catalyst	CO Con. (mol%)	CO-to-CO_2 (mol%)	TOF (min^{-1})	Product distribution (carbon mol%)		
				MeOH	DME	CH_4
Cu@Al_2O_3-dp	25.7	6.5	0.3	5.4	90.4	4.2
Cu@Al_2O_3-im	2.3	0.2	0.1	49.6	14.2	36.2
Cu/Al_2O_3	15.4	4.4	0.2	10.6	63.9	25.5
Cu/Al_2O_3-com	7.9	3.1	0.2	7.3	60.5	32.3

[a] Reaction condition: 0.5 g catalyst, $P = 3.0$ MPa, $T = 260$ °C, $H_2/CO/N_2 = 10/5/5$, $GHSV = 1800$ mL g^{-1} h^{-1}, 2 h of TOS.

ature (about 300–450 °C), corresponding to the desorption of the adsorbed NH_3 on medium acid sites [24,25]. Weak and medium acid sites are identified as the ideal acid active sites for methanol dehydration to dimethyl ether [7]. Moreover, few strong acid sites exist in Cu@Al_2O_3-dp and Cu/Al_2O_3 catalysts. From Fig. S5, it can be observed that Cu@Al_2O_3-dp catalyst has more medium acids and less strong acid than Cu/Al_2O_3, which is beneficial to methanol dehydration and inhibiting the formation of methane and coke [7]. In addition, the Cu@Al_2O_3-im hardly possesses acid sites (2.8 μmol/g), which is attributed to the very low Al content and/or very low surface area. From Table 1, although the Cu@Al_2O_3-dp catalyst shows a slightly lower amount of acidic sites (289.7 μmol/g) than Cu/Al_2O_3 (301.4 μmol/g), it shows much higher DME selectivity (90.4%), resulting from the unique Cu-embedding structure in porous Al_2O_3.

The Cu@Al_2O_3-dp, Cu@Al_2O_3-im and Cu/Al_2O_3 catalysts are applied in the STD reaction, and the results are illustrated in Table 2. Thanks to the unique embedding-type structure and its confinement effect, the Cu@Al_2O_3-dp catalyst shows higher dispersion of Cu, more Cu^+ species and stronger Cu–Al interaction [7,37]. Moreover, the methanol formed on Cu species can only come out through the pore of alumina, during which they are converted to DME by the acidic sites of alumina, and increased the selectivity of DME and decreased the selectivity of methanol, breaking the thermo-dynamically limitation and promoting CO conversion. However, due to the unrestricted and opened reaction environment of conventional supported Cu/Al_2O_3 catalyst, the methanol can be directly desorbed from the catalyst without contacting the acidic site of alumina, which leads to high selectivity of methanol and low selectivity of DME, which inhibits the methanol synthesis reaction and decreases CO conversion. Therefore, the 25.7% of CO conversion and 0.3 min^{-1} of turnover frequency (TOF) are observed over Cu@Al_2O_3-dp, which are much higher than those over the Cu@Al_2O_3-im (2.3%, 0.2 min^{-1}) and Cu/Al_2O_3 (15.4%, 0.2 min^{-1}) catalysts. Meanwhile, Cu@Al_2O_3-dp illustrates much higher distribution of DME (90.4%) compared with Cu@Al_2O_3-im (14.2%) and Cu/Al_2O_3 (63.9%). The selectivity of methanol on the Cu@Al_2O_3-dp is lower than that on the Cu/Al_2O_3, which is ascribed to more medium acidic sites and unique embedded-structure [25]. Moreover, the high selectivity of methane on Cu/Al_2O_3 of 25.5% and Cu@Al_2O_3-im of 36.2% in comparison with 4.2% on the Cu@Al_2O_3-dp can be attributed to the large crystallite sizes of metallic Cu and stronger acidic sites, which are active sites for methanation of CO or decomposition of intermediates such as methanol or possibly DME [7]. For comparison, the supported Cu catalyst on commercial γ-Al_2O_3 with CuO loading of 15.0% was also synthesized (Cu/Al_2O_3-com). The CO conversion and DME selectivity over the Cu/Al_2O_3-com are 7.9% and 60.5%, which are lower than those of the Cu@Al_2O_3-dp and Cu/Al_2O_3. Furthermore, from Table S3 (Supporting information), Cu@Al_2O_3-dp indicates much higher production of DME per hour per gram of CuO than the previously reported Cu-based catalysts. The stability of Cu@Al_2O_3-dp and Cu/Al_2O_3 were measured and are shown in Fig. S6 (Supporting information). It is clear that the CO conversion of Cu@Al_2O_3-dp does not obviously decrease during 28 h of time on stream (TOS). The selectivity of DME over Cu@Al_2O_3-dp catalyst slightly decreases during 28 h, while that over Cu/Al_2O_3 catalyst significantly decreases. A large amount of methane and methanol are produced over the Cu/Al_2O_3 catalyst as time on stream prolongs. From Fig. S6 and Table S4 (Supporting information) the slight decrease of DME selectivity on the Cu@Al_2O_3-dp, compared to Cu/Al_2O_3, results from the loss of a few acidic sites and embedding structure. From Table S4, the loss ratio of acidic sites over Cu@Al_2O_3-dp catalyst is 1.7% during 28 h of time on stream, which is more than Cu/Al_2O_3 catalyst (6.2%).

In this work, a novel Cu-embedded porous Al_2O_3 catalyst has been successfully prepared by filling $Al(OH)_3$ into Cu-BTC framework through the deposition-precipitation followed by a calcination process. The developed Cu@Al_2O_3-dp catalyst displays 25.7% of outstanding CO conversion and 90.4% of DME selectivity in the STD reaction, which are much larger than those over the supported Cu/Al_2O_3 catalyst. Moreover, the Cu@Al_2O_3-dp catalyst also shows higher catalytic stability than Cu/Al_2O_3 catalyst. The outstanding catalytic performance of Cu@Al_2O_3-dp catalyst can be attributed to its unique embedding-type structure, higher Cu dispersion, more Cu^+ species, stronger Cu-Al interaction and more medium acidic sites. This work not only develops a highly efficient catalyst for direct synthesis of DME from syngas, but also provides a new way for designing other embedding-type bifunctional catalysts for diverse consecutive reactions.

Declaration of competing interest

The authors declare no conflicts of interests.

Acknowledgments

This work was financially supported by the National Natural Science Foundation of China (No. U1610104), Liaoning Revitalization Talents Program (No. XLYC1907053, China) and CAS Youth Innovation Promotion Association (No. 2018220, China).

Appendix A. Supplementary data

Supplementary material associated with this article can be found, in the online version, at doi:10.1016/j.cclet.2021.10.031.

References

[1] K. Saravanan, H. Ham, N. Tsubaki, J.W. Ba, Appl. Catal. B: Environ. 217 (2017) 494–522.
[2] E. Catizzone, G. Bonura, M. Migliiori, F. Frusteri, G. Giordano, Molecules 23 (2018) 1–31.
[3] J. Sun, G. Yang, Y. Yoneyama, N. Tsubaki, ACS Catal. 4 (2014) 3346–3356.
[4] Y. Wei, P.E. De Jongh, M.L.M. Bonati, et al., Appl. Catal. A: Gen. 504 (2015) 211–219.
[5] G. Yang, N. Tsubaki, J. Shamoto, Y. Yoneyama, Y. Zhang, J. Am. Chem. Soc. 132 (2010) 8129–8136.
[6] F. Frusteri, M. Cordaro, C. Cannilla, G. Bonura, Appl. Catal. B: Environ. 162 (2015) 57–65.
[7] H. Ham, J. Kim, S.J. Cho, et al., ACS Catal. 6 (2016) 5629–5640.
[8] J. Kampen, S. Booneveld, J. Boon, J. Ventea, M.S. Annaland, Chem. Commun. 56 (2020) 13540.
[9] M. Cai, A. Palčić, V. Subramanian, et al., J. Catal. 338 (2016) 227–238.
[10] F. Li, M. Ao, G.H. Pham, et al., Small 16 (2020) 1906276.
[11] V.V. Ordomsky, M. Cai, V. Sushkevich, et al., Appl. Catal. A: Gen. 486 (2014) 266–275.
[12] X. Zhou, T. Su, Y. Jiang, et al., Chem. Eng. Sci. 153 (2016) 10–20.
[13] A.G. Trenco, E.R. White, M.S.P. Shaffer, C.K. Williams, Catal. Sci. Technol. 6 (2016) 4389–4397.
[14] M. Cai, V. Subramanian, V.V. Sushkevich, V.V. Ordomsky, A.Y. Khodakov, Appl. Catal. A: Gen. 502 (2015) 370–379.
[15] M. Gentzen, W. Habicht, D.E. Doronkin, J.D. Grunwaldt, J. Sauer, Catal. Sci. Technol. 6 (2016) 1054–1063.

[16] S.H. Lima, A.M.S. Forrester, L.A. Palacio, A.C. Faro Jr, Appl. Catal. A: Gen. 488 (2014) 19–27.
[17] Y. Wang, Y. Chen, F. Yu, et al., Energy Chem. 25 (2016) 775–781.
[18] H. Ham, S.W. Baek, C.H. Shin, J.W. Bae, ACS Catal. 9 (2018) 679–690.
[19] K. Takeishi, Y. Wagatsuma, H. Ariga, K. Kon, K. Shimizu, ACS Sust. Chem. Eng. 5 (2017) 3675–3680.
[20] L. Tan, P. Zhang, Y. Suzuki, et al., Ind. Eng. Chem. Res. 51 (2019) 22905–22911.
[21] Y. Wang, W. Wang, Y. Chen, J. Ma, R. Li, Chem. Eng. J. 250 (2014) 248–256.
[22] Y. Sun, X. Han, Z. Zhao, Catal. Sci. Technol. 9 (2019) 3763–3770.
[23] R. Phienluphon, K. Pinkaew, G. Yang, et al., Chem. Eng. J. 270 (2015) 605–611.
[24] Y.L. Guo, Z.K. Zhao, ChemCatChem 12 (2020) 999–1006.
[25] Y.Q. Sun, Z.K. Zhao, ChemCatChem 12 (2020) 1276–1281.
[26] Z. Jin, L. Wang, E. Zuidema, et al., Science 367 (2020) 193–197.
[27] C. Wang, J. Zhang, G. Qin, et al., Chem 6 (2020) 646–657.
[28] M. Du, C. Li, M. Chen, et al., J. Am. Chem. Soc. 136 (2014) 10906–10909.
[29] T. Prasad, D. Hong, M. Suh, Chem. Eur. J. 16 (2016) 14043–14050.
[30] B. An, J. Zhang, K. Cheng, et al., J. Am. Chem. Soc. 139 (2017) 3834–3840.
[31] B. Rungtaweevoranit, J. Baek, J.R. Araujo, et al., Nano Lett. 16 (2016) 7645–7649.
[32] B. Hu, Y. Yin, Z. Zhong, et al., Catal. Sci. Technol. 9 (2019) 2673–2681.
[33] Z. Gu, D. Li, C. Zheng, et al., Angew. Chem. Int. Ed. 56 (2017) 6853–6858.
[34] R.P. Ye, L. Lin, C.C. Chen, et al., ACS Catal. 8 (2018) 3382–3394.
[35] J. Zhuang, D. Ceglarek, S. Pethuraj, A. Terfort, Adv. Funct. Mater. 21 (2011) 1442–1447.
[36] Y. Yao, X. Wu, O.Y. Gutiérrez, et al., Appl. Catal. B: Environ. 267 (2020) 118698.
[37] Y.L. Guo, X.W. Guo, C.S. Song, et al., ChemSusChem 12 (2019) 1–12.
[38] K. Morishige, N.J. Tateishi, Chem. Phys. 119 (2003) 2301–2306.